Mon. Not. R. Astron. Soc. **385,** 1998–2010 (2008) doi:10.1111/j.1365-2966.2008.12908.x

Spectroscopic ages and metallicities of stellar populations: validation of full spectrum fitting

M. Koleva,[1,2⋆] Ph. Prugniel,[1,3] P. Ocvirk,[4,5] D. Le Borgne[4] and C. Soubiran[6]

[1]*CRAL Observatoire de Lyon, CNRS, UMR 5574, ENS de Lyon, Université de Lyon 1, 9 avenue Charles André, F-69230 Saint Genis Laval Cedex, France*
[2]*Department of Astronomy, St Kliment Ohridski University of Sofia, 5 James Bourchier Blvd., BG-1164 Sofia, Bulgaria*
[3]*GEPI, Observatoire de Paris, 61, avenue de l'Observatoire, F-75014 Paris, France*
[4]*Laboratoire AIM, CEA/DSM – CNRS – Université Paris Diderot, DAPNIA/Service d'Astrophysique, CEA-Saclay, 91191 Gif-sur-Yvette, France*
[5]*Astrophysikalisches Institut Potsdam, An der Sternwarte 16, D-14482 Potsdam, Germany*
[6]*Observatoire Aquitain des Sciences de l'Univers, 2 rue de l'Observatoire, 33270 Floirac, CNRS, UMR 5804, France*

Accepted 2007 December 31. Received 2007 December 22; in original form 2007 August 15

ABSTRACT

Fitting whole spectra at intermediate spectral resolution ($R = 1000$–3000), to derive physical properties of stellar populations, appears as an optimized alternative to methods based on spectrophotometric indices: it uses all the redundant information contained in the signal. This paper addresses the validation of the method and it investigates the quality of the population models together with the reliability of the fitting procedures. Our method compares observed optical spectra with models to derive the age, metallicity and line broadening due to the internal kinematics. It is insensitive to the shape of the continuum and the results are consistent with Lick indices but three times more precise. We are using two algorithms: STECKMAP, a non-parametric regularized program and NBURSTS a parametric non-linear minimization.

We compare three spectral synthesis models for single stellar populations (SSPs): Pegase-HR, Galaxev and Vazdekis/Miles, and we analyse spectra of Galactic clusters whose populations are known from studies of colour–magnitude diagrams (CMD) and spectroscopy of individual stars.

We find the following. (1) The quality of the models critically depends on the stellar library they use, and in particular on its coverage in age, metallicity and surface gravity of the stars. Pegase-HR and Vazdekis/Miles are consistent, while the comparison between Pegase-HR and Bruzual & Charlot shows some systematics reflecting the limitations of the stellar library (STELIB) used to generate the latter models. (2) The two fitting programs are consistent. (3) For globular clusters and M67 spectra, the method restitutes metallicities in agreement with spectroscopy of stars with a precision of 0.14 dex. (4) The spectroscopic ages are very sensitive to the presence of a blue horizontal branch (BHB) or of blue stragglers. A BHB morphology results in a young SSP-equivalent age. Fitting a free amount of blue stars in addition to the SSP model to mimic the BHB improves and stabilizes the fit and restores ages in agreement with CMDs studies. This method is potentially able to disentangle age or BHB effects in extragalactic clusters. Full spectrum fitting is reliable method to derive the parameters of a stellar population.

Key words: techniques: spectroscopic – globular clusters: general – Galaxy: stellar content.

1 INTRODUCTION

The goal of this paper is to validate a method for determining the characteristics of a stellar population using an entire medium-resolution spectrum in the rest-frame optical range (rather than concentrating on specific features). Special attention is given to make an optimal use of the information, to look for systematics and to compare the different models of stellar populations.

Stellar populations keep a record of most of the evolution of the stellar systems, and by studying Hertzprung–Russell (HR) diagrams (or colour–magnitude diagrams, CMDs) of galaxies, it is possible to constrain the history of the star formation and enrichment since their formation (see e.g. Grebel 2005). Unfortunately, these star-resolved observations are restricted to nearby galaxies (Local Group and a little further) because of the shallow magnitude limits and

⋆E-mail: mina.koleva@obs.univ-lyon 1.fr

crowding effect. At large distances, only the spectral energy distributions (SED) and the line-of-sight (LOS) integrated spectra are available.

Many methods were devised to determine the age and the metallicity of stellar systems from their integrated light. In this paper we distinguish three approaches.

(i) SED fitting – sensitive to the general shape of the continuum (usually) made in broad wavelength ranges.

(ii) Spectrophotometric indices – concentrates on the strength or equivalent width of specific features, not sensitive to the flux calibration.

(iii) Full spectrum fitting – use all the information by fitting all the pixels, but independently from the shape of the continuum.

SED fitting (Panter, Heavens & Jimenez 2003; Cid Fernandes et al. 2005; Solorio et al. 2005) can be made using colours, low- or medium-resolution spectra. It is performed over large wavelength ranges and compares the observations to models like Pégase.2 (Fioc & Rocca-Volmerange 1997, 1999), Galaxev (Bruzual & Charlot 2003, hereafter BC03) or others. These models should take into account the various sources of extinction (internal and Galactic). SED fitting constrains not only the stellar population but it also informs about the dust content.

Using low- and medium-resolution spectra, the classical approach is to measure spectrophotometric indices, like Lick (Faber 1973; Worthey et al. 1994) or Rose (1984) indices and compare them to model predictions. Spectrophotometric indices measure the strength of some spectral features expected to trace the abundance of particular elements or to correlate with the mean age of stellar populations. However, primarily because a galaxy spectrum is naturally broadened by the internal kinematics, the spectrophotometric indices are defined at low resolution (a few Å) and are therefore blends of many spectral lines. That is why their responses to age and metallicity are quite complex and require careful calibrations (Korn, Maraston & Thomas 2005). Attempts to define indices at a higher resolution (see Le Borgne et al. 2004) require delicate velocity-dispersion corrections or must be designed carefully to reduce their sensitivity to the velocity dispersion. A good example of high-resolution index is the Hγ index defined in Vazdekis & Arimoto (1999). Another possibility to improve the sensitivity of an index to either age or metallicity is to use a composite definition, like for the CaT$*$ (calcium triplet corrected for Paschen lines, Cenarro et al. 2001) or MgFe (insensitive to [α/Fe], González 1993; Thomas, Maraston & Bender 2003) indices.

Lick indices are widely used for more than a decade and the methods continue to improve with introducing the effects of non-solar abundances. However, they use only a few small passbands out of the full observed spectral range, and although the information in the spectrum is probably redundant, this does not optimize the usage of the collected light. Another limitation of the indices is that they are sensitive to missing data or bad pixels (Chilingarian et al. 2007a). The interpolation of spectral bins affected by detector defects or cosmic hits may bias the measurement of the index if the observations are close to the sampling limit. The indices are also affected by weak emission lines (Goudfrooij & Emsellem 1996).

The full spectrum fitting that we propose combines the advantages of spectrophotometric indices and SED fitting. It uses all the information, it is insensitive to extinction or flux calibrating errors and it is not limited by the physical broadening, since the internal kinematics is determined simultaneously with the population parameters. From the point of view of measuring the internal kinematics, it is an extension of the classical methods (e.g. optimal template fitting, van der Marel 1994). The method has been presented in several places (Prugniel et al. 2003; Ocvirk et al. 2006a,b) and its reliability assessed on the basis of various simulations. It is three times more sensitive, but still consistent with Lick indices (Chilingarian et al. 2007a; Michielsen et al. 2007).

Full spectrum fitting is well suited when the resolution is comparable with the physical broadening ($10 < \sigma_{\rm ins} < 200$ km s^{-1}). At lower resolution ($R = 500$–1000) the spectral features are diluted and the sensitivity of the method would rely on the strong spectral features and therefore would become equivalent to Lick indices. At even lower resolution, only strong features, like the Balmer break provides information on the stellar population. In this case, SED fitting using also the shape of the continuum is the good solution.

In its intention to be insensitive to the flux calibration and extinction our full spectrum fitting is close to spectrophotometric indices, but it uses the whole spectrum. A possible disadvantage compared to Lick indices is that the method may, in principle, be sensitive to the wavelength range and to spectral resolution. However, Koleva et al. (2007) have shown that this sensitivity is not critical: the precision of the results mostly depends on the total signal-to-noise ratio (S/N) (i.e. integrated over all the spectral range), and even excluding the Balmer lines does not bias the age determination (only precision is reduced).

To check the reliability of a spectroscopically determined single stellar population (SSP) equivalent age/metallicity, it is wise to test it on globular clusters (GCs) and to compare the results with the results from CMDs determinations. It has been shown (Wolf et al. 2007) that the full spectrum fitting reproduces better the results from the CMDs than the other methods.

This paper is organized as follows. In Section 2 we present the population models and the two algorithms implementing the full spectrum fitting. In Section 3, we use these algorithms to compare different synthetic population models and in Section 4 we invert spectra of Galactic clusters and compare the results with age determinations from HR diagrams. Section 5 discusses the prospects for analysing stellar populations and gives conclusions.

2 POPULATION MODELS AND FITTING METHOD

The goal of this analysis is to retrieve simultaneously the characteristics of the internal kinematics and of the stellar population using a medium-resolution spectrum that integrates along the line of sight the light from a region of a galaxy or cluster (hereafter LOS-integrated spectrum).

The main characteristics of this method are (1) to be insensitive to the shape of the continuum and (2) use all the information in the spectrum. Its principle is to compare an observation to a population model convolved with a LOS velocity distribution (LOSVD). The spectrum of the population model must have the same line spread function (LSF) as the observation (i.e. the LSF of the observation must be injected into the model).

In this section we describe the main ingredients of the method used to analyse stellar populations. First, we present the population models and the stellar libraries used to construct the synthetic spectra. Then we describe the two algorithms used to retrieve the stellar population kinematics and characteristics from the spectra.

2.1 Spectral synthesis models for stellar populations

The population model, i.e. the spectrum corresponding to some formation scenario including a given evolution, is constructed using a population synthesis code. There exists several such codes, and in

this paper we are using Pegase-HR (Le Borgne et al. 2004), Galaxev (BC03) and Vazdekis/Miles (Vazdekis et al. in preparation). These codes differ by their choice of the physical ingredients (IMF, evolutionary tracks, etc.), by the libraries of stellar spectra they are using and by implementation details (in particular interpolations).

2.1.1 *Pegase-HR and ELODIE 3.1*

The Pegase-HR code,[1] as described in Le Borgne et al. (2004), allows a choice of different IMF and different physical ingredients. The evolutionary tracks are from Padova group (Bressan et al. 1993 and companion papers: Padova 94). They are identical to those used for Pegase.2 (Fioc & Rocca-Volmerange 1999). For the present work we use SSPs computed with Salpeter IMF (with lower mass 0.1 $M_{\odot}$ and upper mass 120 $M_{\odot}$).

At variance with Le Borgne et al. (2004), we are using a new version of the ELODIE library[2] (version 3.1; Prugniel et al. 2007a) at a resolution full width at half-maximum (FWHM) = 0.55 Å or $R = \Delta\lambda/\lambda = 10\,000$ at $\lambda = 5500$ Å. The ELODIE library is constructed from the spectroscopic archive of Observatoire de Haute-Provence[3] (Moultaka et al. 2004) and the principle of the data reduction, flux calibration and determination of the atmospheric parameters are described in Prugniel & Soubiran (2001). The set of 1962 spectra of 1388 stars is unchanged in the current release with respect to Prugniel & Soubiran (2004). A comparison between the different theoretical and empirical libraries made by Martins & Coelho (2007b) shows that the coverage of the library in effective temperature, surface gravity and metallicity ($T_{\rm eff}$, log g and [Fe/H]) is one of the best from the present libraries and therefore well suited for population studies (still, enlarging the library towards cooler stars and lower metallicity is desirable, and is currently under preparation).

In the current release, the wavelength range, 3900–6800 Å has been extended in the blue and includes the H&K lines (Fig. 1).

In addition, the data processing and the determination of the atmospheric parameters have been also improved in several ways. In particular, it was found that the diffuse light was undersubtracted by the standard reduction pipeline. This light is normally modelled using the interorder regions, but at the edge of the CCD where the first blue orders are located the diffuse light displays steep variations and is not properly fitted by the model. The undersubtraction of the diffuse light affects the blue region of the spectrum, below about 4400 Å. We applied an ad hoc correction of this effect in order to avoid the full reprocessing from the initial CCD images (see Erspamer & North 2002, for a fine tuned full reprocessing). The blue range, up to about 4400 Å is affected by this small correction.

The comparison of a Pegase-HR SSP with Vazdekis/Miles, Fig. 1, shows that the models are visually consistent even in the blue extremity where ELODIE spectra have lower S/N. It also reveals that the flux calibration of ELODIE is losing precision below 3970 Å. Though it is not critical for our full spectrum fitting method, it may be of importance for other applications. This degradation is due to the sensitivity drop in the blue and to edge effect in the calibration process.

The isochrones used in Pegase-HR are scaled-solar at different values of the total metallicity Z and this has two consequences on the modelling and analysis of stellar populations.

(i) It is well established and understood that the metallic mixture of the Sun is not universal. For example, non-solar abundances of the α elements are surely the explanation of the misfit of a strong spectral feature such as the Mg triplet and MgH band near 5170 Å in elliptical galaxies (Worthey, Faber & González 1992). The GCs are other important environment where the α elements are enhanced, [Mg/Fe] > 0. Therefore, scaled-solar models are not strictly appropriate in those cases, because the location of the isochrones in the HR diagram depends on the detailed chemical composition (Salaris & Weiss 1998; Salasnich et al. 2000; Kim et al. 2002). Age determinations may be biased by up to 20 per cent. At low metallicity ([Fe/H] < -0.7 dex) the location of the isochrones mostly depends on the total metallicity, Z, while at higher metallicity the position of the giant branch is rather controlled by [Fe/H] (but a simple rescaling is not possible). This limitation will be solved only when evolutionary tracks at non solar [α/Fe] will be implemented in Pegase-HR.

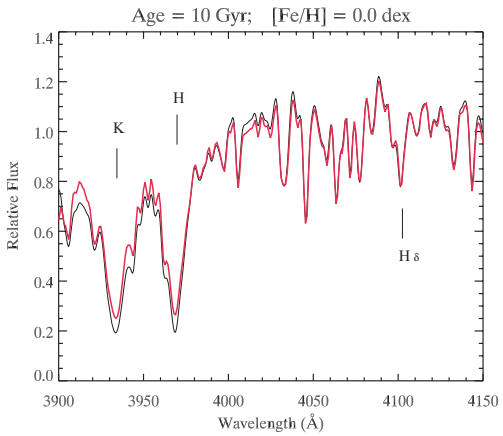

Figure 1. Direct comparison between Pegase-HR/ELODIE.3.1 (in black) and Vazdekis/Miles (in red, thick line) populations of 10 Gyr, solar metallicity in the region of H&K. The Pegase-HR spectrum was convolved by an LSF of 60 km s^{-1} dispersion to match it to the resolution of MILES, the vertical scale was adjusted to have the same flux at 4000 Å.

(ii) The stellar library is constituted from stars of the solar neighbourhood, and though detailed measurements of [α/Fe] are available for only a small fraction of the stars, we can assume that it has the typical abundance pattern of this population (see e.g. Wheeler, Sneden & Truran 1989; [α/Fe] increases when [Fe/H] decreases). In Pegase-HR we neglected the change of [α/Fe] and of Z when [Fe/H] decreases (the predicted spectra have the correct Fe content but have an excess of α elements at low metallicity). This has to be considered when interpreting the metallicities determined using these models.

2.1.2 *Galaxev and the STELIB library*

The Galaxev models (BC03) use a variety of evolutionary tracks: Padova 94 (as Pegase-HR), Padova 2000 (Girardi et al. 2000) and Geneva (Schaller et al. 1992). After comparing these different prescriptions, the authors adopted as 'standard' model the Padova 94 set, because Padova 2000 would predict exaggerately old ages for elliptical galaxies (the red giant branch is 50–200 K warmer in Padova 2000).

These models are build using the STELIB library (Le Borgne et al. 2003), with a resolution ≈3 Å FWHM in the spectral range 3200–9500 Å. STELIB contains 249 spectra but only 187 stars have measured metallicity and can be used to compute the predicted spectra. The coverage in the parameters space is much more limited that in the other recent libraries (see Martins & Coelho 2007b).

[1] http://www2.iap.fr/pegase/pegasehr/.
[2] http://www.obs.u-bordeaux1.fr/m2a/soubiran/elodie_library.html.
[3] http://atlas.obs-hp.fr/elodie.

2.1.3 Vazdekis and the MILES library

Vazdekis/Miles models[4] are based on the previous models from (Vazdekis 1999; Vazdekis et al. 2003). They use Padova 2000 isochrones, which as we pointed before has hotter red giant branch. They cover ages between 0.1 and 17.5 Gyr and metallicities between −1.7 and 0.2 dex. The MILES library Sanchez-Blazquez et al. (2006) used for these models have a 2.3 Å spectral resolution (FWHM) and cover the wavelength range from 3525 to 7500 Å. This library is believed to be better flux calibrated than any other.

2.2 Fitting methods

2.2.1 Pre-treatment: LSF matching

In order to use SSP models to analyse observed spectra, a prior requirement is to match the spectral resolution of the models to that of the observations.

The spectral resolution is coarsely characterized by its FWHM, but entering in the details, the instrumental broadening or LSF (the spectral equivalent of the point spread function for images) is not necessarily a Gaussian and varies with the wavelength and position in the field (for integral field or long-slit spectrographs). Therefore, matching the resolution is not a mere convolution.

Note that we are considering here only the instrumental broadening. Observed spectral features are also broadened by the internal kinematics of the galaxies or clusters, and this *physical* broadening is measured by our analysis method.

The operation proceeds in two steps. First, we determine the LSF and its variation with the wavelength, and then we inject it in the model. To be more precise, we do not need to determine the intrinsic, but simply the relative LSF, i.e. the relative broadening function between the spectrum to analyse and the model.

In principle, when dealing with original observations, the LSF can be determined using some template stars or using twilight spectra (i.e. solar spectrum). But in the present paper where we analyse models and stars clusters from a library, we cannot access such calibrations. Therefore, we measure the total broadening (instrumental plus physical).

To determine the relative LSF we first used the program NBURSTS (see below) to identify the best matching Pegase-HR SSP, and then we measured locally the LSF in 10 overlapping segments of the spectrum with the PPXF program[5] (Cappellari & Emsellem 2004).

The ability to recover kinematical information distinguishes our method from others which either fix the systemic velocity ($v_{\rm sys}$) and the velocity dispersion (σ) or adopt values from independent measurements. In the present case where we analyse models and clusters, with no or very low physical velocity dispersion, we decreased the measured LSF to simulate a physical dispersion of 30 km s^{-1}.

Finally, the population models are convolved by all the local LSFs and interpolated between these convolved segments to reproduce the wavelength variation of the real LSF. The importance of the LSF injection cannot easily be judged from the visual inspection of the residuals between the 'observation' and the best-fitting model, since the fit without this correction appears already excellent. But the effect could be seen on the χ^2 maps: the well in the minimum region becomes sharper with the LSF injection and the estimated error bars decrease.

To compute the values of the χ^2 we are using the following formula: $\chi^2 = [(\text{observation-model})^2/\text{errors}^2]/\text{nfreedom}$, where nfreedom is the number of the pixels in the original data and the errors are sum between the errors in the models and the errors in the observations ($\text{errors}_{\rm models}{}^2 + \text{errors}_{\rm obs}{}^2$). The errors of the observations of GCs are taken from the library of Schiavon et al. 2005. For the errors of the models we adopted S/N = 100 for Vazdekis/Miles and BC03 and 150 for Pegase-HR (from visual inspection of residuals from the fits). These choices affect only the χ^2 scale which should therefore be considered as relative, as values lower than one on some of the maps reported in this paper are demonstrating. Finally to produce χ^2 maps we scan the space of age and metallicity, fitting only the coefficients of LOSVD and multiplicative polynomial and fixing the parameters of the SSPs (t,[Fe/H]).

2.2.2 NBURSTS

The program NBURSTS (see a preliminary description in Chilingarian et al. 2007b) performs a parametric non-linear fit.

The model used in this paper is an SSP convolved with a Gaussian LOSVD and multiplied by a polynomial whose degree is chosen to absorb any flux calibration systematics or effects of extinction:

$$\text{Obs}(\lambda) = P_n(\lambda) \times [\text{SSP}(t, [\text{Fe/H}], \lambda) \oplus \text{LOSVD}(v_{\rm sys}, \sigma, h3, h4)]. \quad (1)$$

The free parameters of the minimization are the characteristics of the SSP – age (t) and metallicity ([Fe/H]); the characteristics of the LOSVD ($v_{\rm sys}, \sigma, h3, h4$), and the $n+1$ coefficients of the multiplicative function P_n, a linear combination of Legendre polynomials.

NBURSTS makes a Levenberg–Marquart minimization and can fit a combination of SSPs or complex stellar population (in this paper we are fitting only SSPs). The population models are spline interpolated over a t − [Fe/H] grid of models (a linear interpolation would not work because the derivatives must be continuous). It is written in IDL/GDL starting from PPXF and uses the MPFIT[6] procedure. The fitting algorithm appears stable, because the free parameters are independent enough, and no additional regularization was required. At low S/N the high-order terms of the LOSVD can be neglected (e.g. fixed to 0).

The degree of the polynomial can be quite large. Experimenting with fits against Pegase-HR models (wavelength range 3900–6800 Å) we found that the results were stable for degrees between 12 and 50. With $n = 50$ and a wavelength range of 3000 Å, the fit can absorb variations in the continuum at the scale of about 60 Å, which is comparable to Lick indices (linearly interpolating the continuum between two side bands). The high-order terms of the multiplicative polynomial are well decoupled from all the kinematical and population parameters. The χ^2 maps with $n = 50$ are more regular and have a sharper and deeper minimum. When two local minima exist, it is easier to identify the absolute one. In principle, at an even higher degree the polynomial should become degenerated with the velocity dispersion and metallicity, but we did not find such an effect (we did not explore degrees higher than 100). The main inconvenient of a high degree is the sensitivity to spikes of emission lines, which should be preliminary masked or clipped using a fit with a low-degree polynomial.

It is important to stress that the inclusion of a multiplicative continuum differs from the 'rectification' of the flux calibration used in some other algorithms, like Mathis, Charlot & Brinchmann (2006) where the spectrum and the model are divided by their top-hat

[4] http://www.ucm.es/info/Astrof/miles/miles.html.

[5] http://www.strw.leidenuniv.nl/∼mcappell/idl/.

[6] Markwardt, http://cow.physics.wisc.edu/∼craigm/idl/idl.html.

filtered versions (width of 500 Å). Since both the observation and the model are similarly filtered the results should not be biased but the sensitivity to the broad molecular bands of MgH, TiO or CN is probably reduced. At variance, our approach does not affect the real spectral features, it is rather similar to the method of Simien & Prugniel (like in Simien & Prugniel 2002) that renormalizes the observations using a polynomial fitted on the ratio between the observation and the best model and iterate until convergence.

2.2.3 STECKMAP

STECKMAP[7] (STEllar Content and Kinematics via Maximum a Posteriori) is a Bayesian method to interpret galaxy spectra in terms of stellar content. It uses a non-parametric formalism, i.e. no shape is assumed a priori for the variables, e.g. the stellar age distribution. Its principles, along with extensive simulations are given in Ocvirk et al. (2006a,b). The algorithm coded in *yorick* is now reasonably user friendly and the package contains some plugged-in SSP models (BC03; Le Borgne et al. 2004; Gonzalez Delgado et al. 2005).

STECKMAP determines age and metallicity distributions (actually weights of the SSPs of the basis). In order to compare with the results of NBURSTS, we compute the luminosity weighted age as

$$t_{\rm lw} = 10^{\sum_{i=1}^{n} X_i \log(t_i)}, \quad (2)$$

where t_i is the age of the ith SSP of the basis and X_i is the weight (i.e. flux fraction) of this component. Similarly, we derive the luminosity-weighted metallicity as

$$[{\rm Fe/H}]_{\rm lw} = 10^{\sum_{i=1}^{n} X_i \log([{\rm Fe/H}]_i)}. \quad (3)$$

These luminosity weighted quantities are expected to be comparable to the SSP-equivalent values determined by other procedures, including NBURSTS, and actually the two types of measurements are often confused in the literature. Note however that 'luminosity-weighted' and 'SSP-equivalent' values are not formally the same; their difference depends on the laws of variation of the luminosity of the continuum and strength of the features with time and metallicity.

In the present paper we are interested in comparing simple populations and will therefore not consider the details of the full stellar age distributions recovered with STECKMAP.

3 ANALYSING ONE POPULATION MODEL WITH ANOTHER ONE AS A REFERENCE

In this section we will compare different models to check their consistency. We will invert SSPs produced by a particular population synthesis code using a grid of models made with a different code, and compare the retrieved population parameters with the nominal ones.

We restricted the comparison to intermediate-age and old populations: 600 Myr–15 Gyr. We do not discuss the younger ages because we do not have reference spectra of real clusters for an external validation. Note however that we noted a counterintuitive dependence of the strength of the metallic lines in young Pegase-HR models. At a given age, lines like Ca at 4227 Å become stronger when the metallicity decreases, as a result of the decreasing temperature of the isochrones. A validation of the analysis of young population should be carried on in a separate future work.

We also excluded the highest bin of supersolar metallicity generated by Pegase-HR which is absent in BC03 and Vazdekis/Miles models.

The metallicity range of the comparisons is $-1.7 < [{\rm Fe/H}] < 0.4$ for BC03 and $-1.7 < [{\rm Fe/H}] < +0.2$ for Vazdekis/Miles. For Vazdekis/Miles and BC03 we use the SSPs given by the authors. The fit was made starting from 4000 Å to be consistent with the fit of the GCs (see Section 4).

[7] http://astro.u-strasbg.fr/Obs/GALAXIES/stecmap_eng.html.

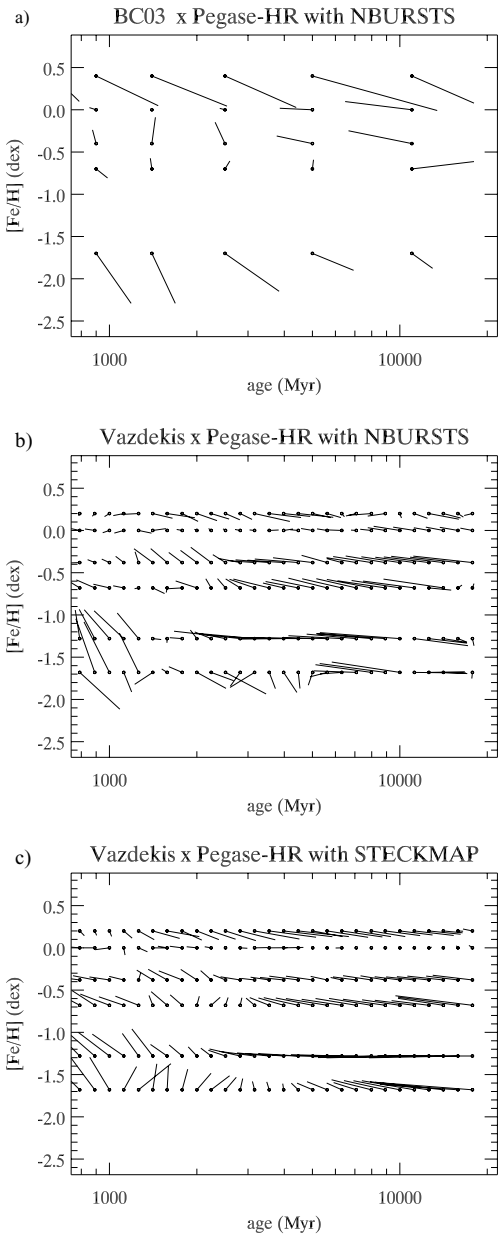

Figure 2. Fits of BC03 with NBURSTS (a), Vazdekis/Miles with NBURSTS (b) and Vazdekis/Miles with STECKMAP (c) SSPs, using Pegase-HR as a reference. Each vector represents an individual inversion. The dots are the location of the nominal characteristics of the population and the tips of the vectors are the values returned by the analysis procedure.

Fig. 2 presents the result of the inversion of both BC03 and Vazdekis/Miles SSPs using a grid of Pegase-HR models. We performed the fit using the two inversion algorithms NBURSTS and STECKMAP.

The BC03 versus Pegase-HR comparison (Fig. 2a) reveals a reasonable consistency for solar metallicity, and for a wide range of ages (from 900 Myr to 11 Gyr). For either subsolar or supersolar metallicity the inversion by Pegase-HR restores characteristics converging towards solar. At metallicity of $[{\rm Fe/H}] = -0.7$ dex the inversion is acceptable, but degrades again in the lowest metallicity bin.

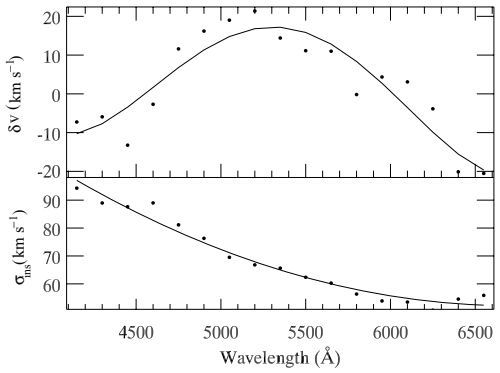

Figure 3. Error of velocity and variation on instrumental velocity dispersion in BC03/STELIB models as a function of the wavelength. The dots represent the measured values and the lines are the polynomial fits with degrees of 4 and 2 for velocity and for dispersion, respectively.

The reasons for these discrepancies can be found in the details of the computation of the BC03 spectra. Indeed, the 187 stars of the BC03 library are strongly concentrated around solar metallicity (one-third of them have $-0.2 <$ [Fe/H] < 0.1) as in most of the other libraries. But the small number of stars remaining at non-solar metallicity makes the modelling hazardous.

To generate a SSP spectrum, BC03 uses the STELIB spectra which are the closest to the isochrone sampling point. In particular, for each metallicity they choose the stars having a compatible [Fe/H]. At solar metallicity the HR diagram is sampled by 69 stars with close-to-solar metallicities. But for [Fe/H] $= 0.4$ dex, the 41 stars that are used have a mean metallicity which is only slightly supersolar. Also, the 69 stars used for the [Fe/H] $= -0.4$ dex bin span a metallicity range from solar to [Fe/H] $= -0.7$ dex with an average close to [Fe/H] $= -0.2$ dex. Not surprisingly, the inversions of the corresponding SSPs in the age range 0.5–10 Gyr reproduce this convergence towards solar metallicity. The [Fe/H] $= -0.7$ dex bin is represented by only 22 stars which are actually well distributed around this median value, and the comparison with Pegase-HR is more consistent. The last metallicity bin of BC03, [Fe/H] $= -1.7$ dex is computed from 25 stars spanning a large range in metallicity, and the comparison with Pegase-HR follows the expected discrepancy.

A direct comparison between BC03 and Vazdekis/Miles gives the same results, hence confirming this analysis. Another weakness of the BC03 models was revealed by our analysis. The inaccurate wavelength calibration of STELIB results in velocity errors up to 40 km s^{-1} (shifts of 0.6 Å; see Fig. 3). The wavelength dependence of the velocity error can be expressed as $\delta v(\lambda) = 8248.5 - 6.5433\lambda + 0.001\,906\lambda^2 - 2.419 \times 10^{-07}\lambda^3 + 1.128 \times 10^{-11}\lambda^4$, and the change of the velocity dispersion as $\sigma_{\rm ins}(\lambda) = 346.620 - 0.0855\lambda + 0.000\,006\lambda^2$, *where* λ is in Å, δv and $\sigma_{\rm ins}$ are in km s^{-1} . δv is relative to ELODIE.3.1 (whose wavelength calibration is very precise), and $\sigma_{\rm ins}$ is the absolute instrumental velocity dispersion deconvolved from the LSF of Pegase-HR (13 km s^{-1}). The LSF for the different SSPs from BC03/STELIB was found consistent despite the inhomogeneous origins of the spectra.

Contrasting with the previous, the comparison between Vazdekis/Miles and Pegase-HR (Figs 2b and c) is considerably more consistent (the MILES library counts almost as many stars as ELODIE.3.1 and has a comparable coverage of the space of parameters). Pegase-HR is using the Padova 94 tracks and Vazdekis/Miles Padova 2000 which, should result in overestimating the SSP-equivalent ages (BC03). The difference between the two sets of isochrones is compatible with the deviations between the two models in Figs 2(b) and (c).

Fig. 4 compares Pegase-HR and Vazdekis/Miles spectra for three representative regions of Figs 2(b) and (c). The two models at the same age and metallicity are overplotted with only adjustment of the velocity dispersion and multiplicative polynomial. The residuals are of the order of 1 per cent, even for the lowest metallicity bin, where the S/N of the libraries is lower because of the few stars in that region.

We also studied the dependence of the solution on the initial guesses given to NBURSTS in order to identify cases where the solution is trapped by a local minimum. In general, the solution is stable for a very wide range of initial guesses and the χ^2 maps (Fig. 5) confirm that there is an unique global minimum.

Only in the region of old age (>10 Gyr) and low metallicity ([Fe/H] ≈ -1.7) the topology of the χ^2 map becomes more complex and the sensitivity to the guesses critical. In this regime the age dependence of most features is small and irregular. It corresponds to the region where the Lick bi-index grids, like H_β versus MgFe, fold on themselves, making age and metallicity determinations ambiguous. This region is of importance for the study of GCs, and we note that unlike Lick indices our method can determine unambiguously the age if care is taken to avoid the secondary minimum (see Section 4.1). Nevertheless, we should also stress two limitations of the models in that region: (i) the stellar libraries are only sparsely populated and (ii) the metallicities are poorly sampled by the isochrones, the two values provided in Padova 94: [Fe/H] $= -1.7$ and -0.7 dex are considerably spaced, and intermediate models are interpolated.

To estimate the effect of the interpolation of the modelled spectra between the metallicities we computed spectra with intermediate metallicities with Pegase-HR (performing linear interpolation) and we inverted them with the standard Pegase-HR grid (NBURSTS makes spline interpolations). The errors are generally negligible (0.009 dex or 2 per cent on age, 0.006 dex on [Fe/H]), except at low metallicity, i.e. between the two widely separated sets of isochrones: [Fe/H] $= -1.2$ dex, where the errors are (0.09 dex or 20 per cent in age and 0.02 dex on [Fe/H]).

4 ANALYSIS OF GALACTIC CLUSTERS

We have shown that (1) full spectrum fitting can recover SSP-equivalent ages and metallicities and (2) the two recent population models are consistent with each others (BC03 has the disadvantage of using sparsely populated library), we want now to assess the reliability of this analysis. For this purpose, we will analyse high-quality spectra of Galactic clusters for which studies of deep CMDs are separately available.

First, we will analyse the 60 spectra from the Schiavon et al. (2005) library of 40 GCs covering a wide range of metallicities. Secondly, we will fit the spectrum of the open cluster M67 from Schiavon, Caldwell & Rose (2004a). The latter object will complement in the high-metallicity and intermediate-age regime the tests made on the GCs (M67 has solar metallicity and is ≈4 Gyr old).

4.1 Globular clusters

The sample of GCs from Schiavon et al. (2005) was observed at a resolution of about 3.1 Å. The observations in the range 3350–6430 Å were done with a long-slit spectrograph in drift-scan mode in order to integrate the population within one core radius. The mean S/N varies from 50 to 240 Å^{-1} depending on the cluster.

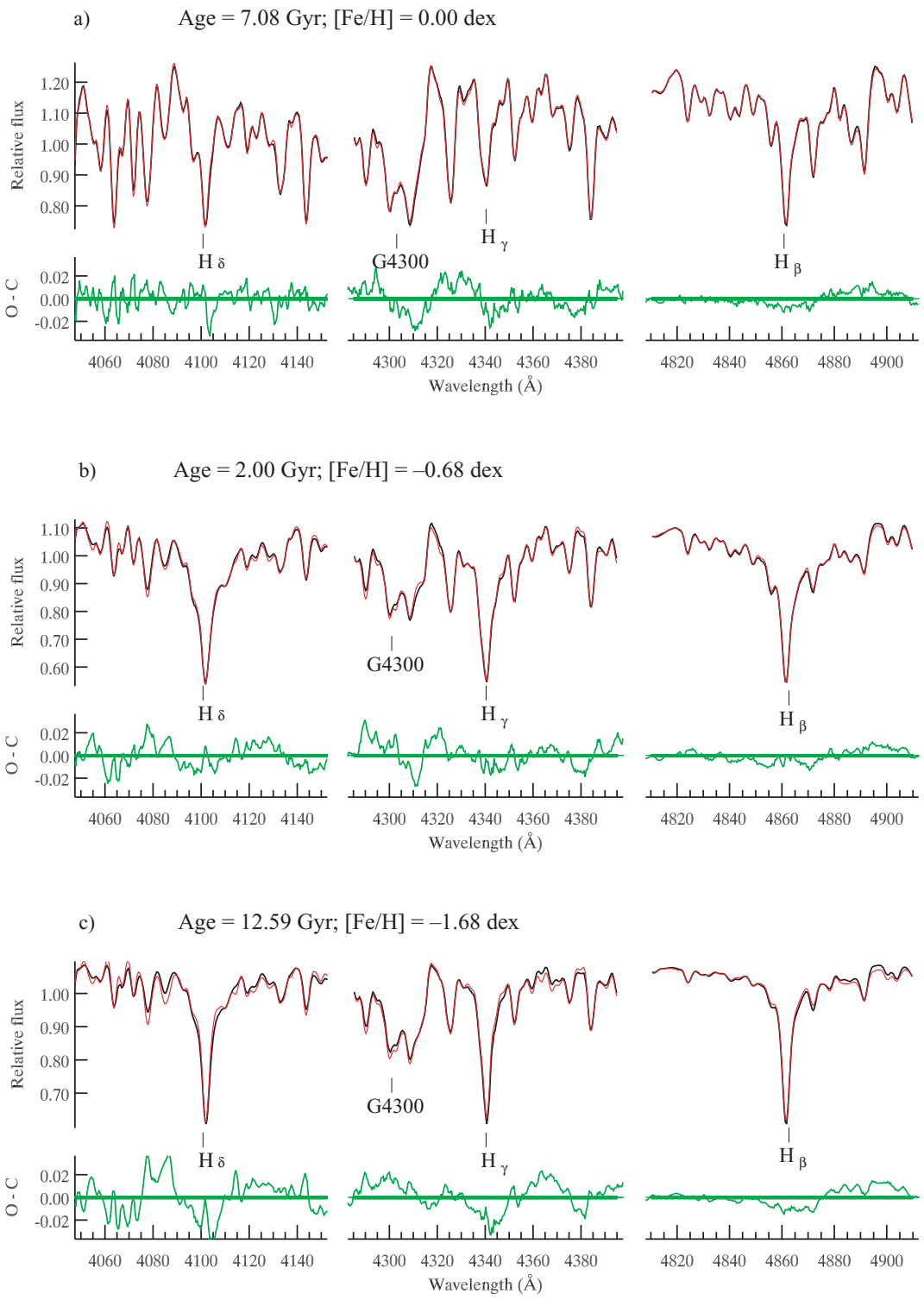

Figure 4. Direct comparison between SSP spectra from Vazdekis/Miles (black line) and the SSPs of Pegase-HR/ELODIE.3.1 (red, thick line). The ages/metallicities of the SSPs are: (a) 7 Gyr/0.0 dex; (b) 2 Gyr/−0.68 dex; (c) 12.6 Gyr/−1.68 dex. The Pegase-HR spectrum was convolved with an LSF of 60 km s^{-1} dispersion to match it to the resolution of MILES. The spectra are normalized to 1. In green (O − C) we show the residuals.

4.1.1 Analysis

The fitting was performed in the wavelength range 4000–5700 Å. We shortened the original spectra to this range because (i) the red part of the observations has poorer quality, due to the correction of telluric lines and its inclusion does not improve the quality of the fit (χ^2 is not decreased) and (ii) when we use also the blue region of the spectrum, including in particular the H&K lines, the quality of the fit is decreased and the results are biased by 1 Gyr towards younger ages. The S/N in this region is lower in

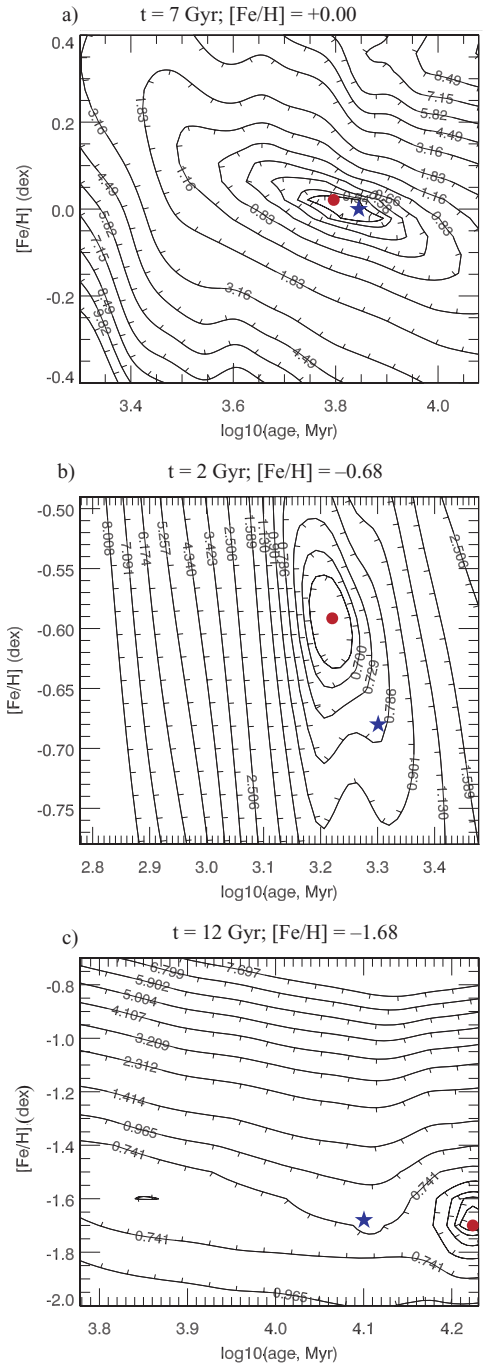

Figure 5. χ^2 maps for the comparison between Vazdekis/Miles and Pegase-HR SSP spectra of Fig. 4 [(a) [Fe/H] = 0.0 dex $t = 7$ Gyr; (b) [Fe/H] = −0.68 dex and $t = 2$ Gyr; (c) [Fe/H] = −1.68 dex, $t = 12.59$ Gyr] inverted with Pegase-HR/ELODIE.3.1. The minimum is shown with a red circle. The blue star corresponds to the age/metallicity of the input SSP. The contours represent the χ^2 isolines.

both the models and the observations, but this does not explain the larger χ^2. The H&K lines are deeper in the models than in the observations. Fig. 1 shows that the Pegase-HR models are still consistent with those of Vazdekis/Miles, and the inversion of the GC observations with the latter reproduce the same problem. If the mismatch comes from the observations, we can suspect a data reduction problem (subtraction of diffuse light) of a characteristics of the cluster population (Ca overabundance; but Ca4227 is well fitted). We did not investigate further this question and we excluded this blue range.

We used the same grid of Pegase-HR model and multiplicative polynomial as in the previous section.

The instrumental velocity dispersion measured from the calibration lamp by Schiavon et al. (2005) varies with wavelength. The instrumental velocity dispersion is quite constant above 5000 Å at about $\sigma_{\rm ins} = 75$–80 km s^{-1} and rise up to over 100 km s^{-1} at 4000 Å. Since this is a sensitive point of our method we redetermined the LSF as explained in Section 3. We found the wavelength calibration to be precise and the high-order moments insignificant, so we only corrected the variation of $\sigma_{\rm ins}$ using the median of the 60 individual LSFs (one per observed spectrum).

When analysing the spectra with NBURSTS we found that at low metallicity the algorithm happens to stop sometimes at a local minimum. We solved this problem starting from different guesses covering ages from 5 to 15 Gyr and appropriate metallicities and we chose the deepest (hopefully absolute) minimum. We discarded solutions older than 15 Gyr, except for NGC 5986 for which there is no minimum younger than that.

At low metallicity the spectral features are not very sensitive to age (see Section 3, Fig. 5). In the bi-index grids, this corresponds to the region where the different isochrones are very close and even cross one another. In our analysis, this results in the local minima found for some clusters. Choosing carefully the initial guess (we are making several fits from a grid of guesses), it is possible to determine the real solution.

The fits for all the observations are presented in graphical form in Appendix A. The χ^2 maps in age and metallicity allow to understand the degeneracies and convergence issues. At the minimum, the χ^2 are in the range 0.63–2.88 and the rms residuals in the whole wavelength range are between 0.6 and 1.9 per cent. χ^2 values lower than one are most probably due to overestimation of the errors in the models.

A close examination of the residuals reveals that the bottom of the modelled Balmer lines is typically 1.9 per cent deeper in the best-fitting models than in the observation (intensity in the centre of the line). Forcing the fit to reduce this departure (i.e. increasing the weight of the Balmer lines) typically leads to an increase of the age by 1 Gyr (i.e. 10 per cent or 0.04 dex). The origin of this mismatch may be either in the models or in the observations. We have the same residuals when fitting with the Vazdekis/Miles models, therefore, if it is not an observational artefact, the reason would have to be investigated in the physical ingredients (evolutionary tracks and IMF). Otherwise, an undersubtraction of the background, could explain the residuals.

Two other features are not fitted precisely. The Mg triplet and MgH band around 5175 Å and the CN band near 4160 Å. This is clearly an effect of the difference between the abundance pattern of the library and the one of the clusters that are α-enhanced compared to the Sun. At high metallicity, the library is scaled-solar and therefore clusters like NGC 6528, 6553 or 6624 have deeper Mg than the best-fitting model. At low metallicity, the library is also α-enhanced (it has the abundance pattern of the solar neighbourhood; see e.g. Wheeler et al. 1989) and the clusters are well fitted (rms ≈ 0.1 per cent). Fig. A1 shows the effect of the abundances for different metallicities. Prugniel et al. (2007b) have shown that using a semi-empirical library it is possible to improve the fit and determine the enhancement.

The CN band near 4150 Å is often misfitted in the GCs because non-solar abundances of C and N. Therefore we masked the region 4145–4155 Å which is about half the central bandpass of the CN1 and CN2 Lick indices.

4.1.2 Results

The results of the fits are presented in Table 1. In Fig. 6(a) we compare the value of [Fe/H] found with our method and the one

Table 1. Comparison of the ages/metallicities obtained with our method and those from the literature. Column 1: ID of the spectra in Schiavon et al. (2005) library consisting in (i) name of the cluster; (ii) (a,b,c) for observations in different nights; (iii) (1,2) for extraction in different apertures. Column 2: the ages, metallicities and corresponding errors from full spectrum fitting with Pegase-HR; column 3: like column 2 but fitting also a fraction of hot stars. Column 4: ages/metallicities/HBR from the literature. The HBR $= (B - R)/(B + V + R)$, is taken from the Harris catalogue (Harris 1996).

	Pegase-HR		Pegase-HR + hot stars		Literature		
Name	age (Gyr)	[Fe/H]	age (Gyr)	[Fe/H]	age (Gyr)	[Fe/H]	HBR
NGC 0104 a 1	10.35 ± 0.31	-0.762 ± 0.006	11.26 ± 0.38	-0.747 ± 0.006	10.7	-0.70^{a}	-0.99
NGC 1851 a 1	5.32 ± 0.11	-1.163 ± 0.007	7.64 ± 0.47	-1.131 ± 0.009	9.2	-1.21^{c}	-0.36
NGC 1904 a 1	11.99 ± 0.57	-1.948 ± 0.012	14.02 ± 0.25	-1.884 ± 0.021	11.7	-1.55^{c}	-0.89
NGC 1904 b 1	14.94 ± 0.14	-1.891 ± 0.011	14.06 ± 0.19	-1.878 ± 0.015			
NGC 2298 a 1	14.44 ± 0.42	-2.033 ± 0.024	13.84 ± 0.56	-1.961 ± 0.033	12.6	-1.97^{a}	0.93
NGC 2298 b 1	10.25 ± 0.63	-2.123 ± 0.018	11.04 ± 0.85	-1.999 ± 0.027			
NGC 2808 a 1	6.77 ± 0.19	-1.155 ± 0.010	8.00 ± 0.41	-1.105 ± 0.007	10.2	-1.29^{c}	-0.49
NGC 2808 b 1	6.92 ± 0.21	-1.161 ± 0.011	7.97 ± 0.32	-1.104 ± 0.008			
NGC 3201 a 1	5.10 ± 0.16	-1.232 ± 0.010	7.68 ± 0.78	-1.195 ± 0.013	11.3	-1.56^{a}	0.08
NGC 3201 b 1	7.04 ± 0.31	-1.351 ± 0.015	10.87 ± 1.19	-1.308 ± 0.015			
NGC 5286 a 1	14.20 ± 0.15	-1.894 ± 0.011	12.47 ± 0.74	-1.730 ± 0.019	12.0	-1.51^{d}	0.80
NGC 5286 b 1	11.93 ± 0.68	-1.882 ± 0.014	12.63 ± 0.79	-1.681 ± 0.022			
NGC 5286 c 1	13.13 ± 0.26	-1.827 ± 0.011	12.50 ± 0.54	-1.519 ± 0.011			
NGC 5904 a 1	5.26 ± 0.10	-1.334 ± 0.007	8.07 ± 0.36	-1.247 ± 0.009	10.9	-1.26^{a}	0.31
NGC 5904 b 1	5.45 ± 0.09	-1.301 ± 0.006	8.22 ± 0.36	-1.226 ± 0.008			
NGC 5927 a 1	9.70 ± 0.35	-0.463 ± 0.011	11.05 ± 0.49	-0.439 ± 0.011	10.0	-0.64^{b}	-1.00
NGC 5927 b 1	11.08 ± 0.51	-0.512 ± 0.011	12.72 ± 0.77	-0.487 ± 0.011			
NGC 5946 a 1	11.45 ± 1.06	-1.794 ± 0.022	12.33 ± 1.24	-1.568 ± 0.025	12.5	-1.54^{d}	1.00
NGC 5986 a 1	15.83 ± 0.11	-1.879 ± 0.012	12.66 ± 0.58	-1.562 ± 0.014	12.0	-1.53^{c}	0.97
NGC 6121 a 1	6.86 ± 0.22	-1.283 ± 0.012	10.91 ± 0.80	-1.227 ± 0.010	11.7	-1.15^{a}	-0.06
NGC 6171 a 1	6.60 ± 0.39	-0.974 ± 0.020	7.98 ± 0.99	-0.956 ± 0.014	11.7	-1.13^{c}	-0.73
NGC 6171 b 1	7.92 ± 0.42	-0.999 ± 0.013	10.58 ± 0.84	-0.974 ± 0.013			
NGC 6218 a 1	7.19 ± 0.23	-1.511 ± 0.012	11.24 ± 0.70	-1.405 ± 0.013	12.5	-1.32^{c}	0.97
NGC 6235 a 1	6.76 ± 0.53	-1.286 ± 0.032	11.21 ± 2.34	-1.268 ± 0.027	12.0	-1.36^{c}	0.89
NGC 6254 a 1	11.74 ± 0.63	-1.770 ± 0.012	12.62 ± 0.63	-1.620 ± 0.016	11.8	-1.51^{a}	0.98
NGC 6266 a 1	6.34 ± 0.18	-1.133 ± 0.009	7.99 ± 0.36	-1.112 ± 0.007	12.0	-1.20^{c}	0.32
NGC 6284 a 1	5.29 ± 0.14	-1.215 ± 0.009	10.42 ± 0.69	-1.160 ± 0.011	12.0	-1.27^{d}	1.00
NGC 6284 a 2	5.30 ± 0.13	-1.152 ± 0.008	8.27 ± 0.46	-1.090 ± 0.010			
NGC 6304 a 1	10.12 ± 0.44	-0.580 ± 0.011	10.39 ± 0.50	-0.566 ± 0.011	10.0	-0.66^{b}	-1.00
NGC 6316 a 1	11.97 ± 0.63	-0.810 ± 0.012	12.51 ± 0.74	-0.799 ± 0.013	10.0	-0.90^{d}	-1.00
NGC 6316 b 1	10.97 ± 0.53	-0.816 ± 0.009	12.47 ± 0.68	-0.804 ± 0.012			
NGC 6333 a 1	14.60 ± 0.22	-2.031 ± 0.013	14.12 ± 0.26	-1.968 ± 0.017	12.0	-1.65^{d}	0.87
NGC 6342 a 1	8.96 ± 0.74	-0.910 ± 0.019	11.43 ± 1.55	-0.920 ± 0.018	12.0	-1.01^{d}	-1.00
NGC 6352 a 1	13.21 ± 0.64	-0.693 ± 0.009	13.25 ± 0.50	-0.693 ± 0.009	9.9	-0.70^{b}	-1.00
NGC 6356 a 1	11.35 ± 0.41	-0.715 ± 0.008	13.14 ± 0.64	-0.706 ± 0.009	10.0	-0.74^{d}	-1.00
NGC 6362 a 1	9.75 ± 0.44	-1.164 ± 0.014	13.18 ± 0.65	-1.102 ± 0.011	11.3	-1.17^{c}	-0.58
NGC 6388 a 1	5.77 ± 0.13	-0.590 ± 0.009	6.54 ± 0.39	-0.550 ± 0.008	10.6	-0.68^{d}	0.00
NGC 6441 a 1	5.92 ± 0.15	-0.544 ± 0.010	6.88 ± 0.41	-0.522 ± 0.008	12.7	-0.65^{d}	0.00
NGC 6441 a 2	5.95 ± 0.15	-0.544 ± 0.009	6.77 ± 0.22	-0.520 ± 0.008			
NGC 6522 a 1	5.24 ± 0.14	-1.117 ± 0.008	8.07 ± 0.49	-1.051 ± 0.010	12.0	-1.39^{c}	0.71
NGC 6528 a 1	11.10 ± 0.39	-0.279 ± 0.010	13.29 ± 0.57	-0.239 ± 0.009	10.0	-0.10^{c}	-1.00
NGC 6528 a 2	10.88 ± 0.34	-0.268 ± 0.009	11.98 ± 0.39	-0.230 ± 0.009			
NGC 6528 b 1	8.75 ± 0.29	-0.218 ± 0.012	11.56 ± 0.55	-0.206 ± 0.012			
NGC 6528 b 2	8.83 ± 0.26	-0.213 ± 0.011	11.04 ± 0.43	-0.202 ± 0.011			
NGC 6528 c 1	11.35 ± 0.43	-0.306 ± 0.011	14.15 ± 0.66	-0.264 ± 0.010			
NGC 6528 c 2	11.85 ± 0.44	-0.291 ± 0.009	11.85 ± 0.44	-0.291 ± 0.009			
NGC 6544 a 1	13.55 ± 0.32	-1.333 ± 0.011	12.99 ± 0.64	-1.251 ± 0.012	12.7	-1.38^{c}	1.00
NGC 6553 a 1	8.71 ± 0.24	-0.284 ± 0.010	14.05 ± 0.66	-0.252 ± 0.009	10.0	-0.20^{c}	-1.00
NGC 6569 a 1	15.00 ± 0.51	-1.028 ± 0.009	13.65 ± 0.87	-0.960 ± 0.013	10.9	-1.08^{d}	-0.51
NGC 6624 a 1	8.14 ± 0.26	-0.698 ± 0.009	8.21 ± 0.31	-0.692 ± 0.009	10.6	-0.70^{b}	-1.00
NGC 6624 a 2	8.30 ± 0.26	-0.701 ± 0.008	8.35 ± 0.29	-0.700 ± 0.008			
NGC 6626 a 1	5.52 ± 0.12	-1.234 ± 0.007	12.78 ± 0.53	-1.179 ± 0.009	12.0	-1.21^{c}	0.90
NGC 6637 a 1	12.96 ± 0.54	-0.857 ± 0.007	13.14 ± 0.61	-0.841 ± 0.007	10.6	-0.78^{b}	-1.00
NGC 6638 a 1	9.92 ± 0.43	-0.966 ± 0.011	13.14 ± 0.75	-0.936 ± 0.009	11.5	-1.08^{c}	-0.30

Table 1 – *continued*

Name	Pegase-HR age (Gyr)	Pegase-HR [Fe/H]	Pegase-HR + hot stars age (Gyr)	Pegase-HR + hot stars [Fe/H]	Literature age (Gyr)	Literature [Fe/H]	HBR
NGC 6652 a 1	10.52 ± 0.36	−0.999 ± 0.007	11.27 ± 0.63	−0.988 ± 0.008	11.4	−1.10[d]	−1.00
NGC 6652 b 1	8.65 ± 0.33	−1.061 ± 0.007	11.26 ± 0.73	−1.087 ± 0.008			
NGC 6723 a 1	7.29 ± 0.24	−1.299 ± 0.011	10.75 ± 0.90	−1.278 ± 0.011	11.6	−1.14[c]	−0.08
NGC 6752 a 1	8.63 ± 0.25	−1.933 ± 0.013	12.60 ± 0.82	−1.864 ± 0.022	12.2	−1.57[a]	1.00
NGC 7078 a 1	10.42 ± 0.45	−2.291 ± 0.000	10.56 ± 0.54	−2.279 ± 0.017	12.0	−2.26[d]	0.96
NGC 7078 a 2	10.49 ± 0.39	−2.291 ± 0.000	10.59 ± 0.47	−2.255 ± 0.015			

[a][Fe/H] from Kraft & Ivans (2003); [b][Fe/H] from Carretta & Gratton (1997); [c][Fe/H] from Carretta & Gratton (1997), corrected by −0.18 dex (see Schiavon et al. 2005); [d][Fe/H] from Schiavon et al. (in preparation).

from Schiavon et al. (2005); the standard deviation between the two series of determinations is 0.17 dex. The reference ages are taken mainly from Salaris & Weiss 2002; Santos & Piatti 2004; Krusberg & Chaboyer 2006, for the clusters for which we did not find age reference we adopted values of 10 Gyr.

The distribution of the ages (Fig. 6b) appears more spread than those determined from CMD analyses for which the dispersion is ≈2 Gyr. The effects that can alter the age determinations are (1) contamination of the spectrum by field stars, and (2) the horizontal branch morphology.

Contamination by field stars may only be important in some rare cases and in particular for the bulge GCs (like e.g. NGC 6553).

The horizontal branch morphology or existence of blue stragglers are well known to affect the spectroscopic determination of the ages (de Freitas Pacheco & Barbuy 1995; Lee, Yoon & Lee 2000; Maraston & Thomas 2000). The horizontal branch morphology, i.e. the colour distribution of the stars of the horizontal branch, primarily depends on the metallicity. The most metal poor clusters have generally the larger blue extension of the HB. But it presents broad variations (the so-called second-parameter problem, see Recio-Blanco et al. 2006 for a recent discussion) weakly correlated with other properties of the clusters (density, luminosity, etc.). This presence of old blue stars (helium-burning core) mimics an intermediate/young age population. However, Schiavon et al. (2004b), revisiting this question with the spectra of the data base used in the present paper, have shown the ability to constrain the blue horizontal branch (BHB) contribution from the integrated light spectra using Fe sensitive line and the ratio between H_β and H_δ.

In Figs 6 and 7 the clusters are separated in two groups according to the value of the horizontal branch ratio, HBR $= (B - R)/(B + V + R) < -0.5$ (Harris 1996). We adopted the limit between the red and the blue HB morphology clusters at HBR > -0.5 in order to attach clusters like NGC 2808 (HBR $= -0.49$, Harris 1996) known to have blue tail (Castellani et al. 2006) to the 'blue' group. Since our models do not reproduce the HB morphology, the clusters with blue HB tend to have younger ages.

We included the effect of blue HB as an additional component in our model. We fitted a non-negative linear combination between the SSP(t,[Fe/H]) and a set of stars in the temperature range from 6000 to 20 000 K. This new fit returns also the contribution of each star in the best-fitting mix. These additional parameters are adding more parameters to the fit. The consequence is that the space of parameters is more degenerated. However, the overall χ^2 values are a little bit smaller when hot stars are added. Fig. 7 shows that the ages of the blue clusters are moved by about 4 Gyr (0.20 dex), while the other clusters are less affected (0.07 dex). Only five (from 40) blue HB morphology clusters are left with an age younger than 8 Gyr. Also the metallicities are in better agreement with the metallicities from Schiavon et al. (2005), the standard deviation is 0.14 dex. In Fig. 8 we are showing the dependence of the light fraction of the hot star in the best-fitting model on HBR. There is a tendency to have a larger fraction of hot stars when the HBR increases (e.g. more blue stars).

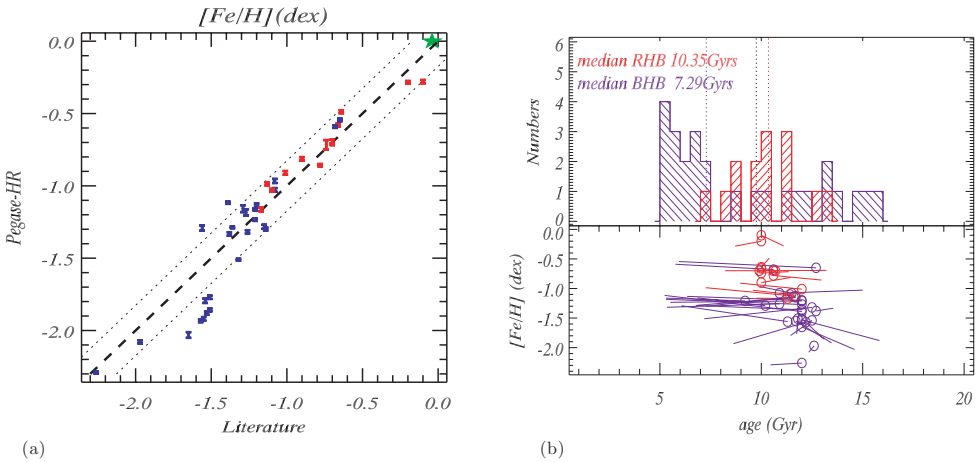

Figure 6. Relations for the GCs. (a) Comparison between the metallicities found with NBURSTS and those from Schiavon et al. (2005) (spectroscopy of individual stars). The dotted lines represent 1σ deviation. The green star represents M67. (b) The upper panel shows the histogram of the ages. The dotted lines represent the median age for the clusters; the lower panel compares the ages and metallicities that we find and those from the literature. The circles show the positions from the literature and the end of the vectors are our estimations. Everywhere blue represents the clusters with BHB and red represents the other clusters.

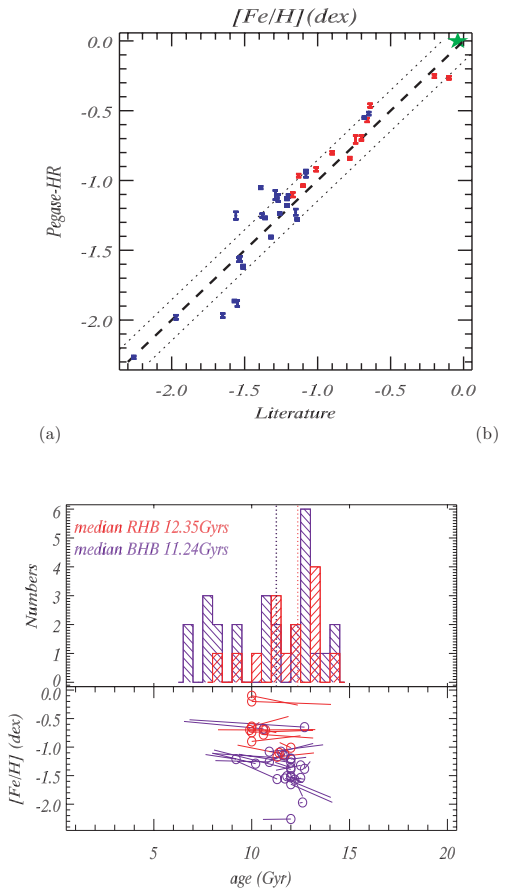

Figure 7. Same as Fig. 6, but the fit was made adding hot stars component to the SSPs models to account for the contribution of BHB.

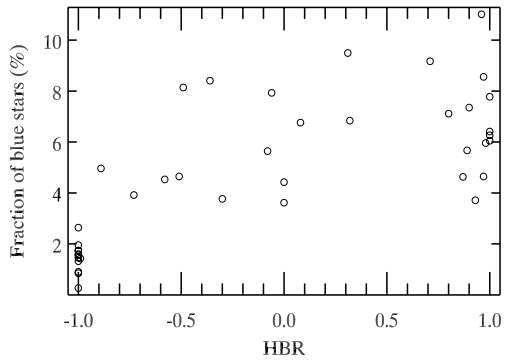

Figure 8. Light fraction of hot stars used by the best-fitting model as a function of the HBR of the clusters. As expected, the fraction of hot stars increases with the HBR.

4.2 M67

The Galactic open cluster, M67, is an interesting case to complete the comparison with the clusters since it contains an intermediate-age and metal-rich population quite similar to many diffuse elliptical galaxies (see e.g. Michielsen et al. 2007) or to M32.

We are using the spectrum presented in (Schiavon et al. 2004a) and assembled from spectra of individual stars in the clusters (and of some nearby dwarfs to replace the M67 dwarfs which are too faint to be observed). The Pegase-HR fit of M67 is shown in Fig. 9.

The SSP-equivalent age 2.90 ± 0.02 Gyr and metallicity [Fe/H] = −0.033 ± 0.006 dex are close to those determined by spectrophotometric indices from the same spectrum (3.5 ± 0.5 Gyr and [Fe/H] = 0.00 dex, Schiavon et al. 2004a) and compatible with the characteristics obtained from CMD analysis (Salaris & Weiss 2002; Santos & Piatti 2004).

In this high-metallicity regime, the models are of the best quality as also shown in the comparisons of Section 3, and the stellar libraries sample ideally the corresponding region of atmospheric parameters. For low luminosity elliptical galaxies, we can consider our full spectrum fitting method as highly reliable.

5 CONCLUSIONS

We investigated the consistency and the reliability of the determination of SSP-equivalent age and metallicity of stellar populations using full spectrum fitting. Our method, suited to analyse medium-resolution ($R > 1000$) spectra, compares an observation to a model to derive the parameters of the stellar population and the kinematical shifting and broadening.

We found a precise agreement between the Pegase-HR and Vazdekis/Miles models. For metallicities greater than −1.0 dex and ages between 600 Myr and 15 Gyr the metallicities of the models agree to 0.064 dex and ages to 15.5 per cent (0.060 dex). At low metallicity ([Fe/H] < −1.4 dex) and intermediate to old ages, the age sensitivity is poor, and care must be taken to avoid local minima.

The BC03 models present systematic biases that are probably due to the poor metallicity coverage of the STELIB library. The main pattern is that they 'overestimate' the metallicity of their models for [Fe/H] > 0 dex and they 'underestimate' the metallicity of their models for −1 < [Fe/H] < 0.

Turning to real data, we found a good agreement between the SSP-equivalent age and metallicity of M67 (2.9 Gyr and −0.03 dex) with those derived from spectrophotometric indices and from CMD analysis. Regarding the GCs, the mismatch of Mg and CN due to non-solar abundances does not prevent a reliable determination of [Fe/H]. The comparison with metallicity measurements from the paper of Schiavon et al. (2005) indicate rms([Fe/H]) = 0.14 dex.

The main difficulty in the interpretation of the integrated spectra of GCs, is the determination of the ages. In particular the horizontal branch morphology, or presence of blue stragglers can significantly alter the ages to misleadingly young value. The Pegase-HR SSPs do not model the horizontal branch morphology and for blue morphology the fits with NBURSTS returns ages underestimated by up to 30–50 per cent. With STECKMAP the BHB are identified as a young (⩽300 Myr) burst. For the other clusters, we find a mean age of 10.4 Gyr with a dispersion of 2.4 Gyr. Including hot stars in the NBURSTS fit to represent the BHB, the age of the blue clusters are restored correctly and the red clusters are less affected. This ability to robustly measure the age of the clusters is potentially very interesting for the study of extragalactic clusters.

In a conclusion, as long as the population can be considered as a single burst, the full spectrum fitting can reliably be used to determine ages and metallicities. It appears particularly robust for the intermediate-age populations of high metallicity ($1 < t < 10$ Gyr, $-1 <$ [Fe/H] < 0).

The full spectrum fitting uses the redundancy of the information distributed along the whole spectrum and it is not possible to identify particular features which constrain either the age or the metallicity. Surely, the Balmer lines are the best age indicators, but we have shown Koleva et al. (2007) that the age can be retrieved even if they are masked. In the present work each wavelength point is weighted

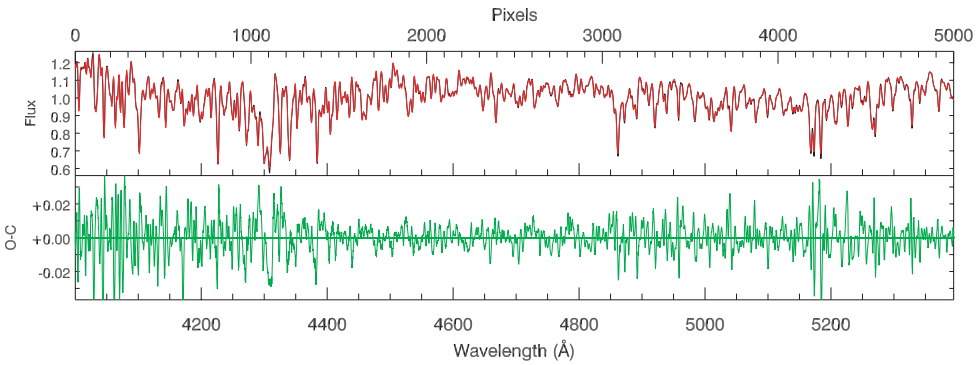

Figure 9. The upper panel displays the spectrum of M67 (Schiavon et al. 2004a). The lower panel shows the residuals from the fit with Pegase-HR and NBURSTS. Note that the vertical scale for the residuals is 10 times expanded with respect to the plot of the spectrum.

according to its uncertainty and we did not intend to modulate the weight of the specific spectral features according to their age or metallicity sensitivity (as in Panter et al. 2003). We may in the future investigate this aspect.

Another important issue for this method is the mismatch due to abundance differences, and in particular to α element enhancement. The present population models are tied to the abundance pattern of the solar neighbourhood and cannot fit the high-metallicity GCs and the elliptical galaxies. But purely theoretical libraries (see Martins & Coelho 2007a), or semi-empirical ones (Prugniel et al. 2007b) will soon allow to build models with variable abundances.

ACKNOWLEDGMENTS

The PhD grant of Mina Koleva has been provided by the French ministry of foreign affairs (Bourse d'excellence Eiffel doctorat). MK acknowledges the support of the Bulgarian National Science Research Fund by the grant F-201/2006. DLB thanks the Centre National d'Etudes Spatiales for its financial support. We are grateful to I. Chilingarian, N. Bavouzet and P. Blondé for their contributions to the development and tests of NBURSTS. We thank James Rose and Ricardo Schiavon for valuable discussions and for providing their data on the Galactic clusters. We thank the anonymous referee for his/her constructive comments.

REFERENCES

Bruzual G., Charlot S., 2003, MNRAS, 344, 1000 (BC03)
Cappellari M., Emsellem E., 2004, PASP, 116, 138
Carretta E., Gratton R. G., 1997, A&AS, 121, 95
Castellani V., Iannicola G., Bono G., Zoccali M., Cassisi S., Buonanno R., 2006, A&A, 446, 569
Cenarro A. J., Gorgas J., Cardiel N., Pedraz S., Peletier R. F., Vazdekis A., 2001, MNRAS, 326, 981
Chilingarian I. V., Prugniel P., Sil'Chenko O. K., Afanasiev V. L., 2007a, MNRAS, 376, 1033
Chilingarian I. V., Prugniel Ph., Sil'Chenko O. K., Koleva M. V., 2007b, in Vazdekis A., Peletier R. eds, Proc. IAU Symp. 241, Stellar Populations as Building Blocks of Galaxies. Cambridge Univ. Press, Cambridge, p. 175
Cid Fernandes R., Mateus A., Sodré L., Stasińska G., Gomes J. M., 2005, MNRAS, 358, 363
de Freitas Pacheco J., Barbuy B., 1995, A&A, 302, 718
Erspamer D., North P., 2002, A&A, 383, 227
Faber S., 1973, ApJ, 179, 731
Fioc M., Rocca-Volmerange B., 1997, A&A, 326, 959
Fioc M., Rocca-Volmerange B., 1999, preprint (astro-ph/9912179)
Girardi L., Bressan A., Bertelli G., Chiosi C., 2000, A&AS, 141, 371
González J., 1993, PhD thesis, Univ. California
Gonzalez Delgado R. M., Cervino M., Martins L. P., Leitherer C., Hauschildt P. H., 2005, MNRAS, 357, 945
Goudfrooij P., Emsellem E., 1996, A&A, 306, L45
Grebel E., 2005, in Jerjen H., Binggeli B. eds, Proc. IAU Symp. 198, Near-fields Cosmology with Dwarf Elliptical Galaxies. Cambridge Univ. Press, Cambridge, p. 1
Harris W., 1996, AJ, 112, 1487
Kim Y., Demarque P., Yi S. K., Alexander D. R., 2002, ApJS, 143, 499
Koleva M., Bavouzet N., Chilingarian I., Prugniel P., 2007, in Kissler-Patig M., Walsh J. R., Roth M. M., eds, ESO Astrophys. Symp., Science Perspectives for 3D Spectroscopy. Springer-Verlag, Berlin, Heidelberg, p. 153
Korn A. J., Maraston C., Thomas D., 2005, A&A, 438, 685
Kraft R. P., Ivans I. I., 2003, PASP, 115, 143
Krusberg Z. A. C., Chaboyer B., 2006, AJ, 131, 1565
Le Borgne J.-F. et al., 2003, A&A, 402, 433
Le Borgne D., Rocca-Volmerange B., Prugniel Ph., Lançon A., Fioc M., Soubiran C., 2004, A&A, 425, 881
Lee H.-C., Yoon S., Lee Y., 2000, AJ, 120, 998
Maraston C., Thomas D., 2000, ApJ, 541, 126
Martins L., Coelho P., 2007a, in Vazdekis A., Peletier R. eds, Proc. IAU Symp. 241, Stellar Populations as Building Blocks of Galaxies. Cambridge Univ. Press, Cambridge, p. 58
Martins L., Coelho P., 2007b, preprint (arXiv:0705.1994)
Mathis H., Charlot S., Brinchmann J., 2006, MNRAS, 365, 385
Michielsen D. et al., 2007, ApJ, 670, L101
Moultaka J., Ilovaisky S. A., Prugniel Ph., Soubiran C., 2004, PASP, 116, 693
Ocvirk P., Pichon C., Lançon A., Thiébaut E., 2006a, MNRAS, 365, 46
Ocvirk P., Pichon C., Lançon A., Thiébaut E., 2006b, MNRAS, 365, 74
Panter B., Heavens A. F., Jimenez R., 2003, MNRAS, 343, 1145
Prugniel Ph., Soubiran C., 2001, A&A, 369, 1048
Prugniel Ph., Soubiran C., 2004, preprint (astro-ph/0409214)
Prugniel Ph. et al., 2003, in Perez E., Gonzalez Delgado R. M., Tenorio-Tagle G., eds, ASP Conf. Ser. Vol. 297, Star Formation Through Time. Astron. Soc. Pac., San Francisco, p. 281
Prugniel Ph., Soubiran C., Koleva M., Le Borgne D., 2007a, preprint (astro-ph/0703658)
Prugniel Ph., Koleva M., Ocvirk P., Le Borgne D., Soubiran C., 2007b, in Vazdekis A., Peletier R., eds, Proc. IAU Symp. 241, Stellar Populations as Building Blocks of Galaxies. Cambridge Univ. Press, Cambridge, p. 68
Recio-Blanco A., Aparicio A., Piotto G., de Angeli F., Djorgovski S., 2006, A&A, 452, 875
Rose J. A., 1984, AJ, 89, 1238
Salaris M., Weiss A., 1998, A&A, 335, 943
Salaris M., Weiss A., 2002, A&A, 388, 492
Salasnich B., Girardi L., Weiss A., Chiosi C., 2000, A&A, 361, 1023

Sanchez-Blazquez P. et al., 2006, MNRAS, 371, 703
Santos J. F. C. Jr, Piatti A. E., 2004, A&A, 428, 79
Schaller G., Schaerer D., Meynet G., Maeder A., 1992, A&AS, 93, 269
Schiavon R. P., Caldwell N., Rose J. A., 2004a, AJ, 127, 1513
Schiavon R., Rose J., Courteau S., MacArthur L., 2004b, ApJ, 608, 33
Schiavon R., Rose J., Courteau S., MacArthur L., 2005, ApJS, 160, 163
Simien F., Prugniel Ph., 2002, A&A, 384, 371
Solorio Th., Fuentes O., Terlevich R., Terlevich E., 2005, MNRAS, 363, 543
Thomas D., Maraston C., Bender R., 2003, MNRAS, 339, 897
van der Marel R. P., 1994, MNRAS, 270, 271
Vazdekis A., 1999, ApJ, 513, 224
Vazdekis A., Arimoto N., 1999, ApJ, 525, 144
Vazdekis A., Cenarro A. J., Gorgas J., Cardiel N., Peletier R. F., 2003, MNRAS, 340, 1317
Wheeler J. C., Sneden C., Truran J. W. Jr, 1989, ARA&A, 27, 279
Wolf M. J., Drory N., Gebhardt K., Hill G. J., 2007, ApJ, 655, 179
Worthey G., Faber S., González J., 1992, ApJ, 398, 69
Worthey G., Faber S., González J., Burstein D., 1994, ApJS, 94, 687

SUPPLEMENTARY MATERIAL

The following supplementary material is available for this article:

Appendix A. In this appendix we present the fit of the 60 spectra of the GCs.

This material is available as part of the online article from: http://www.blackwell-synergy.com/doi/abs/10.1111/j.1365-2966.2008.12908.x (this link will take you to the article abstract).

Please note: Blackwell Publishing are not responsible for the content or functionality of any supplementary materials supplied by the authors. Any queries (other than missing material) should be directed to the corresponding author for the article.

This paper has been typeset from a TEX/LATEX file prepared by the author.